Pore network microarchitecture influences human cortical bone elasticity during growth and aging

Yohann Bala, Emmanuelle Lefèvre, Jean-Paul Roux, Cécile Baron, Philippe Lasaygues, Martine Pithioux, Valérie Kaftandjian, Hélène Follet

Pore network microarchitecture influences human cortical bone elasticity during growth and aging

Yohann Bala[a,b,n], Emmanuelle Lefèvre[c,d], Jean-Paul Roux[b], Cécile Baron[c,d], Philippe Lasaygues[e], Martine Pithioux[c,d], Valérie Kaftandjian[a], Hélène Follet[b]

[a]Laboratoire Vibrations Acoustique, INSA Lyon, Campus LyonTech la Doua, 69621 Villeurbanne Cedex, France
[b]INSERM UMR 1033, Université de Lyon, 69372 Lyon Cedex 08, France
[c]Aix-Marseille University, CNRS, ISM UMR 7287, 13009 Marseille, France
[d]APHM, Institute for Locomotion, Sainte-Marguerite Hospital, 13009 Marseille, France
[e]Laboratory of Mechanics and Acoustics, UPR CNRS 7051, Aix-Marseille University, Centrale Marseille, 13009 Marseille, France

Cortical porosity is a major determinant of bone strength. Haversian and Volkmann's canals are'seen' as pores in 2D cross-section but fashion a dynamic network of interconnected channels in 3D, a quantifiable footprint of intracortical remodeling. Given the changes in bone remodeling across life, we hypothesized that the 3D microarchitecture of the cortical pore network influences its stiffness during growth and ageing.

Cubes of cortical bone of 2 mm side-length were harvested in the distal 1/3 of the fibula in 13 growing children (mean age $\pm$ SD: 13 $\pm$ 4 yrs) and 16 adults (age: 75 $\pm$ 13 yrs). The cubes were imaged using desktop micro-CT (8.14 μm isotropic voxel size). Pores were segmented as a solid to assess pore volume fraction, number, diameter, separation, connectivity and structure model index. Elastic coefficients were derived from measurements of ultrasonic bulk compression and shear wave velocities and apparent mass density.

The pore volume fraction did not significantly differ between children and adults but originates from different microarchitectural patterns. Compared to children, adults had 42% ($p=0.033$) higher pore number that were more connected (Connective Density: +205%, $p=0.001$) with a 18% ($p=0.007$) lower pore separation. After accounting for the contribution of pore volume fraction, axial elasticity in traction-compression mode was significantly correlated with better connectivity in growing children and with pore separation among adults.

The changes in intracortical remodeling across life alter the distribution, size and connectedness of the channels from which cortical void fraction originates. These alterations in pore network microarchitecture participate in changes in compressive and shear mechanical behavior, partly in a porosity-independent manner. The assessment of pore volume fraction (i.e., porosity) provides only a limited understanding of the role of cortical void volume fraction in its mechanical properties.

*Corresponding author at: INSERM UMR_S 1033, 7-11 Rue Guillaume Paradin, 69372 Lyon Cedex 08, France.
E-mail address: yohannbala@gmail.com (Y. Bala).

1. Introduction

Human cortical bone displays a multiscale porous architecture originating from optimization to contradictory needs. Bone has to be stiff and strong to resist loading but light to allow mobility (Bala et al., 2015; Seeman and Delmas, 2006). During last decade, cortical porosity has emerged as a major predictor of bone strength (Baron et al., 2007; McCalden et al., 1993) and fragility fracture (Bala et al., 2014b, 2015; Bjornerem et al., 2013). The cortical void volume fraction contributes to bone mechanical behavior because the apparent density (inverse of porosity) is inversely proportional to the 7th power of its stiffness (Schaffler and Burr, 1988).

Cortical bone void volume originates from Haversian and Volkmann's canals that contain bone vasculature and innervation. While these canals are 'seen' as pores in cross-section images (Chappard et al., 2013; Thomas et al., 2006), they form a three dimensional network of interconnected canals (Chappard et al., 2013; Cooper et al., 2007). The structure of this porous network is not static; the number of canals, their diameter, and their connectedness are the quantifiable footprints of the bone remodeling activity and balance (Cooper et al., 2007).

During growth, the skeleton adapts its size, shape and material properties to be of sufficient strength to support the evolving physical activity (Currey and Butler, 1975; Jee and Frost, 1992; Loro et al., 2000; Palacio-Mancheno et al., 2014; Parfitt et al., 2000). Histomorphometric studies highlighted that this adaptation was made possible through changes in modeling and remodeling activity and its balance at both the tissue and the Bone Multicellular Unit (BMU) level (Parfitt et al., 2000; Rauch et al., 2007). For instance, from 2 to 20 years, the thickening of the cortex is determined by a net positive balance at the tissue level between endocortical resorption and periosteal formation (Rauch et al., 2007). In this age range, intracortical remodeling activation frequency decreases and displays a ~5% positive balance at BMU level reducing intracortical porosity and participating to bone consolidation (Parfitt, 1994b, Parfitt et al., 2000).

During young adulthood, remodeling is slow and in steady-state at the tissue-level - the number of Bone Multicellular Units (BMU) resorbing bone equals the number of BMU refilling cavities excavated earlier at other locations. At the level of the BMU, remodeling is balanced – each BMU resorbs and deposits similar volumes of bone matrix. At this stage there is little or no bone loss or structural decay in cortical bone (Bala et al., 2014a; Compston, 2011). After midlife in women and later in men, a rapid extent of remodeling surfaces at the tissue level coupled to a ~5% negative balance at the BMU level, increases pore number and diameter resulting in an overall higher cortical void volume fraction and permanent bone loss (Bjornerem et al., 2011; Lips et al., 1978; Qiu et al., 2010; Recker et al., 2004; Vedi et al., 1983). This has been repeatedly observed using 2D histomorphometry (Lips et al., 1978; Rauch et al., 2007; Schnitzler, 2015; Schnitzler and Mesquita, 2013; Schnitzler et al., 2009; Zebaze et al., 2010). However, the structural changes in pore network 3D microarchitecture beyond these alterations in the void volume fraction are not known.

Recent studies suggest that porosity achieved during growth may influence intracortical remodeling and structural decay later in life (Bala et al., 2014b; Bjornerem et al., 2013; Bui et al., 2013; Loro et al., 2000; Seeman, 2008). Haversian and Volkmann's canal density, size and connectivity in young adult defines indeed the extent of surfaces available for unbalanced remodeling to be initiated upon at the onset of age-related perturbation at the BMU level (Bui et al., 2013). However, porosity is only regarded as a single value describing void volume fraction and may not be sufficient to predict entirely the influence of microstructure on cortical bone fragility (Chappard et al., 2013; Yeni et al., 1997; Yeni and Norman, 2000). There is most likely a contribution of age-related structural changes in pore network microarchitecture but these parameters, especially in growing bone, are rarely investigated.

Given the age related-changes in bone remodeling activity and balance across life, we hypothesized that cortical bone void volume fraction originates from canals networks with different microarchitectures in growing children and adults. This study also aimed to evaluate comprehensively the impact of the canal network microarchitecture on cortical bone elasticity. We tested these hypotheses in human cortical bone samples collected in the distal fibula of growing children and ageing adults. Pore number, diameter, connectivity and other morphological parameters of the cortical void volume were quantified using micro-CT. These variables were compared to the elasticity assessed in the same samples using ultrasonic bulk wave velocities in the three principal directions of bone. Understanding the contribution of pore volume fraction and pore network microarchitecture to bone mechanical properties during growth and ageing may help in finding early predictors of bone fragility.

2. Material and methods

2.1. Specimens

Bone samples were collected in the distal 1/3 of the fibula in 13 children (9 males and 4 females, mean age $\pm$ SD: 13.2 $\pm$ 3.5 years, range: 6–18 years) during corrective surgery after a fracture at the growth plate or equinovarus of the foot ($n=2$). Equinovarus of the foot is apparently not associated with alterations in bone remodeling parameters (Rauch et al., 2007). Surgeries were performed at the Timone Hospital (Marseille, France). All children were ambulatory prior to surgery and none received medications known to affect bone remodeling. In accordance with the French code of public health and after approbation of the study by the committee for the protection of persons, informed consents were obtained from children's legal guardians. In addition, bone samples were harvested in the distal 1/3 of the fibula from 16 human donors (7 males and 9 females, mean age $\pm$ SD: 75.0 $\pm$ 12.9 years, range: 50–91 years). Autopsies were performed between 2010 and 2012 under the guidance of the INSERM UMR-S 1033 (Lyon, France) and the IFSTTAR UMR-T 9406 (Bron, France) in order to build a bone sample bank. Samples were maintained frozen at $-20\,^{\circ}C$ wrapped in Phosphate Buffer Saline soaked gauze. Twenty-nine 2x2x2

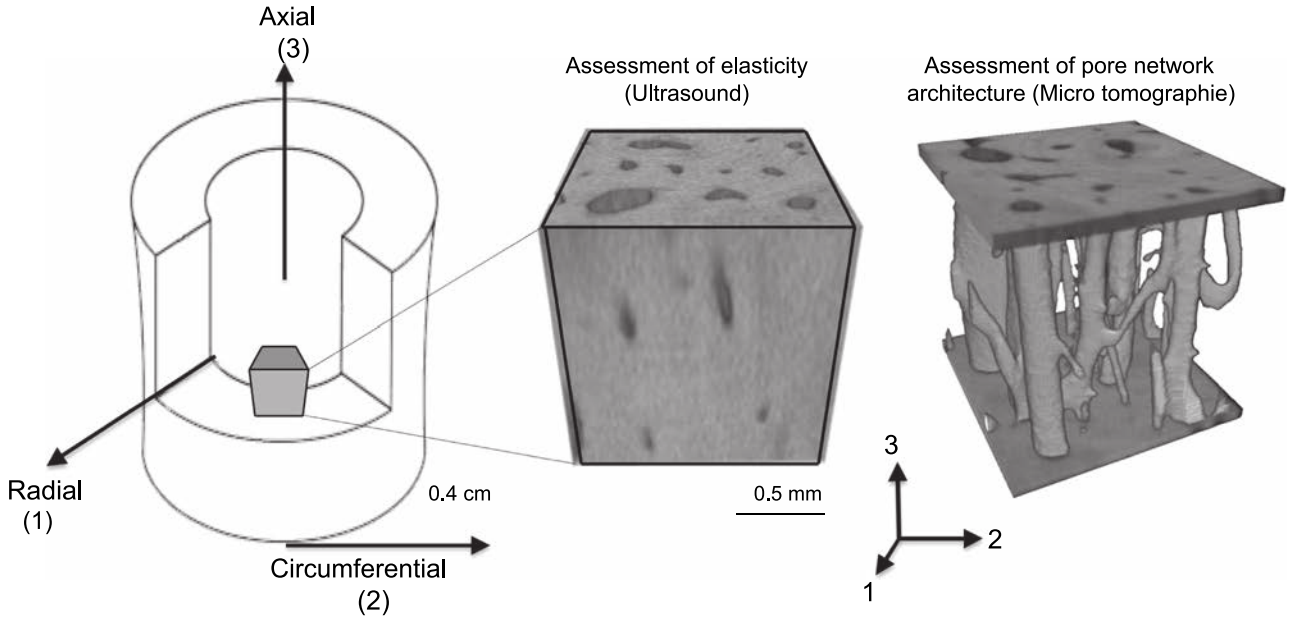

Fig. 1 – From left to right, bone cubical samples were cored from the distal fibula and oriented according to the radial (1), circumferential (2) and axial (3) axes for assessment of the elastic coefficients by ultrasound and pore network architecture using micro-CT.

mm cubic samples were extracted from the cortex using a water-cooled low speed diamond saw (Buehler Isomet 4000, Buehler, Lake Bluff, IL, USA). All cubes included the periosteal region and the 2 mm thickness permitted to avoid the highly 'trabecularized' endosteal region in samples from elderly. The regions of coring were matched by the quadrant and the fraction of bone length between children and adults. Cubes faces were identified according to the radial (axis 1), tangential (axis 2) and axial (axis 3) orientations in the fibula (Fig. 1).

2.2. Image acquisitions

The cubic samples were imaged using a desktop micro-CT system (Skyscan 1174, Bruker, Kontich, Belgium). Scanning was done with the bone specimen immerged in distilled water in a 6 mm inner diameter plastic tube and held in place thanks to gauze. Sample axial axis (i.e., Haversian canals' principal orientation) was aligned to the rotation axis of the sample holder. Scans were performed with a field of view of 1024×1024 pixels a source voltage 50 kV, current 800 μA, rotation step 0.6° over a 360° rotation and a 0.5 mm-thick aluminium filter for beam hardening reduction. An isotropic voxel size of 8.14 μm was used with an exposure time of 4 seconds, 2 frames averaging leading to a total scan time of 82 minutes for each sample. The images were reconstructed using a filtered back-projection algorithm (NRecon software, V 1.6.9, Skyscan NV, Kontich, Belgium). For each cube, a stack of 210 sections was reconstructed.

2.3. Morphometric analysis

From the stack of contiguous reconstructed images, the volumes of interest were selected for morphometric analysis using a semi-automated method (CTAnalyser Software V 1.14.4, Skyscan NV, Kontich, Belgium). For each specimen, the external borders were contoured by the operator and then automatically interpolated over the axial axis defining the volume of interest (VOI). Within the tissue volume (TV, mm^3), the porosity (void volumes) was segmented as a solid and the mineralized bone as a background by using global thresholding. Calibration was performed using a phantom of hydroxyapatite rods, a cut-off of 0.79 g/cm^3 was chosen after observation of several reconstructed images from samples spreading the whole age-range. The following morphometric variables were calculated: the pore volume fraction (Po.V/TV, %), the pore surface to pore volume ratio (Po.S/Po.V, 1/mm). Pore diameter (Po.Dm, μm) corresponding to the average diameter of the pores and pore separation (Po.Sp, μm) corresponding to the average separation between pores were both calculated using a sphere-fitting algorithm (Hildebrand and Ruegsegger, 1997; Ulrich et al., 1999). As an index of heterogeneity in the intra-individual distribution of pore size and separation, the standard deviation of Po.Dm and Po.Sp are reported as Po.Dm.SD and Po.Sp.SD both expressed in μm. The pore number (Po.N, 1/mm) was calculated as: $Po.N = 1/(Po.Sp + Po.Dm)$. Connectivity (ConnD, $1/mm^3$) was evaluated by the Euler characteristic according to the method detailed by Odgaard (1997) and normalized by the TV. We also assessed the pore pattern factor (Po.Pf in analogy with the trabecular pattern factor, 1/mm) calculated as the ratio of volumes and surfaces before and after dilation. Lower Po.Pf indicates higher concavity i.e., better-connected pore network.

2.4. Ultrasound based measurement of bone elasticity

Bone elasticity was determined using a well-established method based on the measurements of ultrasonic bulk compression and shear wave velocities and sample apparent mass density (Espinoza Orias et al., 2009; Granke et al., 2011). This method provides measurements of the elastic properties in the

Table 1 – Values of microstructural parameters of the pore network and elastic coefficients. P-values for group comparison were obtained using Man–Whitney's U test. Bold font denotes p-values r0.05.

	Children (5–18 yrs) Mean (SD)	**Adults (50–91 yrs)** Mean (SD)	P-Value
Po.V/TV (%)	10.3 (6.5)	15.9 (10.3)	0.151
Po.S/Po.V (1/mm)	40.5 (15.9)	37.7 (13.4)	0.628
Po.N (1/mm)	0.69 (0.28)	0.98 (0.29)	**0.033**
Po.Dm (μm)	139 (62)	144 (69)	0.626
Po.Dm.SD (μm)	67 (39)	67 (41)	0.953
Po.Sp (μm)	397 (58)	325 (62)	**0.007**
Po.Sp.SD (μm)	125 (22)	100 (20)	**0.010**
ConnD ($1/mm^3$)	6.6 (5.5)	20.1 (15)	**0.001**
Structure Model Index	3.2 (0.6)	2.8 (0.2)	**0.002**
Po.Pf (1/mm)	0.021 (0.007)	0.017 (0.006)	0.076
Elastic coefficients (Gpa)			
C11	16.1 (2.5)	17.9 (3.6)	**0.021**
C22	15.3 (2.5)	17.9 (6.15)	**0.045**
C33	23.6 (4.4)	28.8 (5.1)	**0.011**
C44	4.1 (0.8)	4.8 (0.6)	**0.017**
C55	4.0 (0.9)	4.9 (1.1)	**0.019**
C66	3.0 (0.4)	3.6 (1.0)	**0.017**

three principal directions of a same bone material volume. The apparent mass density (ρ, g/cm^3) was measured with a micrometric balance equipped with a density kit (Voyager 610, Ohaus Corporation, FlorhamPark, NJ, USA, measurement uncertainty of 0.001 g/cm^3) and the dimensions were measured with a digital caliper (Absolute digimatik solar, Mitutoyo, Kanagawa, Japan, measurement error of 0.03 mm). Taking into account average values of mass densities, determined during the experiments, equal to 1700 kg/m^3, we obtain a relative error of 0.06%. For Time-Of-Flight measurements, uncertainties are of around 0.02 μs, given by the laboratory test apparatus/electroacoustic device (Eurosonic, Vitrolles, France). Given the apparent density ρ, the diagonal terms $C_{ij\ (1 \le i \le 6)}$ of the elastic tensor are calculated from:

$$C_{ii} = \rho.v_{ii}^2 (i = 1, 2, 3)$$

$$C_{44} = \rho.v_{23}^2 = \rho.v_{32}^2$$

$$C_{55} = \rho.v_{13}^2 = \rho.v_{31}^2$$

$$C_{66} = \rho.v_{12}^2 = \rho.v_{21}^2$$

where the longitudinal elastic coefficients C_{11}, C_{22}, and C_{33} represent the stiffness in traction-compression mode, C_{44}, C_{55}, C_{66} represent the shear stiffness coefficients (Fig. 1). Velocity v_{ij} denotes velocity of a wave propagating in the i direction, with particle motion in the j direction. For compressional waves, $i=j$, and for shear waves, $i \neq j$. Compressional and shear waves velocities were measured using a pulse transmission method with a pair of 5 MHz transducers (VP1093, CTS Valpey Corporation, Hopkinton, MA, USA for compressional waves and Panametrics V156, Inc., Waltham, MA, USA for shear waves). The received signal was post-processed with a custom MatLab program (The Mathworks Inc., Natick, MA, USA) (Lefevre et al., 2015). Repeated measurements on a set of same samples revealed a good reproducibility for the stiffness with coefficient of variation ranging between 0.8% and 2.5% depending on the coefficients.

2.5. Statistics

Data are reported as mean ± SD unless otherwise stated. As our population is composed of growing children and ageing adults, all analyses were performed separately in the two groups and not on the pooled population. Statistical analyses were performed using SPPS 20.0 (IBM, Amonk, NY, USA). Normality was tested using Shapiro-Wilk procedure. Most of the variables were not normally distributed, non-parametric test were consequently used. Differences between groups were tested using Mann-Whitney U test. Bivariates correlations between morphometric variables and age were tested by the Spearman's rank correlation test (r'). Correlations between morphometric variables and elastic coefficients were calculated with or without accounting for the contribution of the pore volume fraction. A two-tailed significance level of 0.05 was used.

3. Results

3.1. Pore volume fraction originates from different microarchitectures in children and adults

The pore volume fraction (Po.V/TV) did not significantly differ between growing children and adults but originated from different microarchitectural pattern (Table 1). Relative to children, adults had a higher pore number (Po.N: +42%) and connectivity density (ConnD: +205%), a lower pore separation (Po.Sp: −18%) and intra-individual distribution of separation (Po.Sp.SD: −20%). In accordance with a higher ConnD in adults, Pore pattern factor tended to be lower in adults compared to children but the difference did not reach significance level (Po.Pf: −19%, $p=0.076$) (Table 1).

Table 2 presents the correlation coefficients obtained between the age and the parameters of the pore network microarchitecture. Among growing children, increasing age was negatively correlated with Po.V/TV. This decrease in the pore volume fraction was associated with a decrease in Po.N, Po.Dm and an increase in Po.Sp. Between 5 and 18 years old there was also a positive correlation between age and the specific surface of the pore (Po.S/Po.V). As expected, among adults, increasing age between 50 and 91 years old was correlated with higher Po.V/TV. This increase in pore volume fraction was associated with an increasing Po.N and a decreasing Po.Sp (Fig. 2).

3.2. Pore network microarchitecture contributes to cortical bone elasticity

Despite the differences in pore network microarchitecture, cortical bone from both children and adults were both transversely isotropic (with $C_{33} > C_{11} = C_{22}$ and $C_{44} = C_{55} > C_{66}$). However, relative to children all elastic coefficients were higher in adults (+11%, +17% and +22% for C_{11}, C_{22} and C_{33}, respectively,

and +17%, +23% and +20% for C_{44}, C_{55} and C_{66}, respectively) (Table 1).

Among growing children, increasing age was associated with increasing elastic coefficients in traction-compression. In adult group, increasing age was associated with lower elastic coefficients in traction-compression mode. Correlation between age and shear elastic coefficients did not reach statistical significance in both groups (except for C_{44} in adult group, $r' = -0.70$) (Table 2).

Table 3 reports the correlation coefficients obtained between the elastic coefficients and the parameters of the pore network microarchitecture. Among the children samples, the C_{33} elastic coefficient (i.e., axial traction-compression) was negatively correlated with Po.V/TV, Po.N and Po.Dm (r' from -0.46 to -0.82) and positively Po.S/Po.V, Po.Sp and Po.Pf (r' from 0.48 to 0.88). Similar results were obtained with C_{66} (transverse shear). The positive correlation between C_{33} and Po.Pf remained significant after adjustment for Po.V/TV (r'-adjusted=0.52, p=0.020). In the adult group, C_{33} was negatively correlated with Po.V/TV ($r' = -0.63$) and Po.N ($r' = -0.59$) and positively with Po.Sp ($r' = 0.71$) and Po.Sp.SD ($r' = 0.72$). No correlation was observed between C_{66} and pore network microarchitecture. When accounting for the contribution of Po.V/TV, the correlation between C_{33} and Po.Sp and Po.Sp.SD remained significant (r'-adjusted=0.56, p=0.007 and r'-adjusted=0.70, p=0.001, respectively).

Table 2 – Spearman correlation coefficients (r^0) obtained between variables of the pore network architecture, elastic coefficients and age among children and adults group. Bold font denotes p-values r0.05.

	Children (5–18 yrs)		Adults (50–91 yrs)	
	r′	*p*-value	r′	*p*-value
Po.V / TV (%)	−0.53	**0.043**	0.50	**0.047**
Po.S / Po.V (1/mm)	0.51	**0.048**	−0.19	0.471
Po.N (1/mm)	−0.57	**0.027**	0.53	**0.035**
Po.Dm (μm)	−0.50	**0.048**	0.17	0.524
Po.Dm.SD (μm)	−0.41	0.083	0.23	0.395
Po.Sp (μm)	0.50	**0.049**	−0.77	**0.001**
Po.Sp.SD (μm)	0.58	**0.029**	−0.78	**0.001**
ConnD (1/mm^3)	−0.33	0.232	0.23	0.389
Structure Model Index	−0.15	0.590	−0.23	0.436
Po.Pf (1/mm)	0.62	**0.013**	−0.60	**0.009**
Elastic coefficients (Gpa)				
C11	0.53	**0.022**	−0.41	0.057
C22	0.67	**0.003**	−0.46	**0.038**
C33	0.44	**0.050**	−0.55	**0.014**
C44	0.15	0.292	−0.70	**0.001**
C55	0.17	0.273	−0.22	0.210
C66	0.29	0.151	−0.22	0.207

4. Discussion

To our knowledge, the present study is the first to evaluate the 3D-microarchitecture of the pore network in both children and adults in appendicular skeleton. In site- and size-matched samples of compact-appearing cortex, we report that cortical porosity originates from different canal network microarchitectures in growing children and adults. Growth was associated with a decrease in cortical void volume fraction due to a decrease in pore diameter, pore number and pore connectivity. On the opposite, in adults, ageing was associated with an increase in void volume fraction related to an increase in pore number and pore connectivity, not in pore size. Within the limitations of a small sample size that may results in low statistical power to detect statistical significance for some differences, our data support that elastic properties are influenced by pore network microarchitecture even after accounting for void volume fraction contribution, suggesting an independent contribution.

4.1. Pore network microarchitecture during growth

During growth, long bones increase in width by periosteal apposition (modeling formation) and endocortical resorption (modeling resorption) and in length by endochondral ossification (Cadet et al., 2003; Enlow, 1962; Rauch, 2012). At the same time, bone also undergoes Haversian remodeling to adapt to the mechanical environment and to face the increasing need in calcium (Parfitt, 1994b; Parfitt et al., 2000). Our knowledge of growth-related changes in cortical

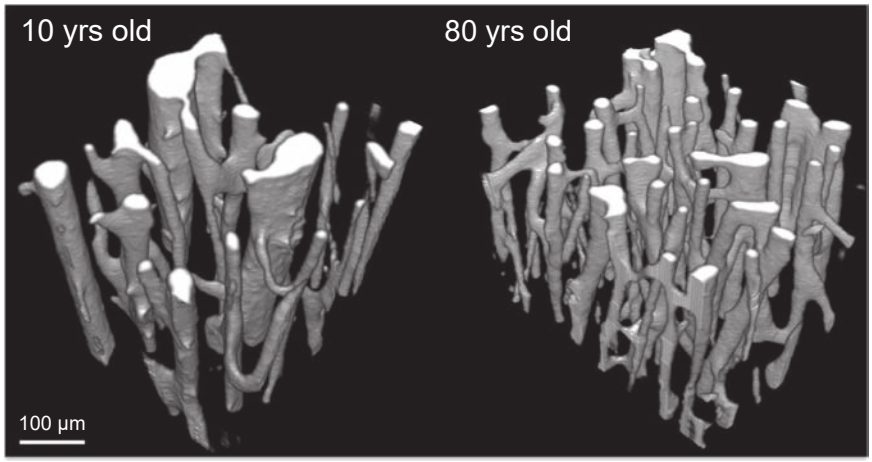

Fig. 2 – 3D reconstructions of the pore network imaged in cube of cortical bone cored in the distal part of the fibula in females.

Table 3 – Spearman correlation coefficients (r^0) obtained between the different variables describing the pore network microarchitecture and the elastic coefficients obtained by ultrasound in children/adults. [n] po0.05, [nn] po0.001, [nnn] po0.0001. a: significant correlation after controlling for the contribution of the void volume fraction (Po.V/TV).

	Elastic coefficients (GPa)											
	C11		C22		C33		C44		C55		C66	
	Children	Adults	Children	Adults	Children	Adults	Children	Adults	Children	Adults	Children	Adults
Po.V/TV (%)	−0.52*	−0.64*	−0.52*	−0.71**	−0.80***	−0.63*	−0.52*	−0.72**	−0.56*	−0.08	−0.65*	−0.13
Po.S/Po.V (1/mm)	0.40	0.69*	0.41	0.66*	0.70*	0.38	0.52*	0.56*	0.50*	0.01	0.64*	0.08
Po.N (1/mm)	−0.80*** [1]	−0.21	−0.72**,[1]	−0.36	−0.82***	−0.59*	−0.55*	−0.67*	−0.60*	−0.25	−0.61*	−0.12
Po.Dm (μm)	−0.23	−0.67*	−0.17	−0.61*	−0.46*	−0.30	−0.55*	−0.64*	−0.30	−0.15	−0.56*	−0.13
Po.Dm.SD (μm)	−0.35	−0.70*,[1]	−0.11	−0.63*	−0.10	−0.41	−0.16	−0.72**	0.02	−0.13	−0.48	−0.16
Po.Sp (μm)	0.62*,[1]	0.32	0.51*	0.50*	0.48*	0.71**,[1]	−0.05	0.70**	0.09	0.14	0.22	0.24
Po.Sp.SD (μm)	0.35	0.24	0.28	0.54*	0.07	0.72**,[1]	−0.55*	0.76**,[1]	−0.32	0.15	0.03	0.41
ConnD ($1/mm^3$)	−0.05	−0.31	−0.38	−0.59*,[1]	−0.39	−0.17	−0.06	−0.20	−0.22	0.37	−0.13	−0.07
Po.Pf (1/mm)	0.61*	0.71**	0.63*,[1]	0.67*	0.88***,[1]	0.49	0.50*	0.63*	0.62*,[1]	0.06	0.69*	−0.10

* $p<0.05$,
** $p<0.001$,
*** $p<0.0001$
[1] $p<0.05$ after controlling for the contribution of Po.V/TV

porosity has been nurtured by histomorphometric studies performed in iliac crest samples limiting comparison with present results. Most of these studies reported a high porosity in children principally originating from large asymmetrical drifting osteons (Schnitzler and Mesquita, 2013). In this set up, bone resorption not only progresses in the cutting cone forming a round and narrow canal in the matrix, but also toward the endosteal surface. In these units, the onset of bone formation appears to be delayed forming canals up to 30 times larger than common cutting cones (Robling and Stout, 1999; Schnitzler and Mesquita, 2013). Later when growth slowdowns, these asymmetrical osteons are replaced through remodeling by smaller symmetrical concentric osteons (Parfitt, 1994a; Schnitzler, 2015; Schnitzler and Mesquita, 2013).

We propose that the age-related decrease in void volume fraction we observed might also be due to the replacement of large drifting osteons by smaller symmetrical osteons. Our bone samples were not evaluated by histomorphometry. However, in the context of this study, we collected fibula samples from a 6 years old and 16 years old boys and imaged them using microradiography (Montagner et al., 2015). The resulting images supported our statement and suggested a transition from large asymmetric drifting osteons to smaller symmetric osteons during growth at the fibula (Fig. 3). Growth has been associated with an age-dependent decrease in remodeling frequency. Rauch et al. indeed highlighted a fall in the percentage of active osteons from ~70% at 5 years old to ~20% at 20 years old (Rauch et al., 2007). These mechanisms contract the remodeling space consolidating bones (Parfitt et al., 2000; Schnitzler et al., 2009).

In the present study, the consolidation of the cortical bone (*i.e.*, suggested by an increase in C_{33}) was not only associated with the decrease in porosity but also with an increase in the pore pattern factor. This suggests that in growing children, the age-related decrease in pore network connectivity also increases stiffness in axial direction. However, as observed for most of the variables describing pore network microarchitecture, correlations were stronger with the elastic coefficients corresponding to the tension-compression mode than in shear. This may indicate that shear elasticity is more sensitive to different parameters of cortical structure other than porosity or material properties. Indeed, several *ex vivo* studies show alterations of bone tissue structure and composition at the micro- and nano-scale during growth. Akkus et al. suggested that the remaining fraction of primary lamellar bone continues to mature as they observed an increase in mineral particles size and an improvement in its crystallinity between 17 and 25 years (Akkus et al., 2003). Saito et al., described also age-related changes in average collagen enzymatic cross-linking profile with a transition from the immature forms to mature ones (Saito and Marumo, 2010). All these parameters of bone quality are known determinants of bone mechanical behavior in human adults and in animal models (see (Bala and Seeman, 2015; Ural and Vashishth, 2014) for reviews). Finally, it has been shown in rats cortical bone that Young's and shear moduli derived from ultrasounds were not determined by the same physicochemical properties. For instance, shearing was influenced by crystal size while elasticity was principally determined by apparent density (Kohles and Martinez, 2000). Taken together, these results suggest that cortical shear and tensile-compressive stiffness may not be similarly sensitive to growth-related changes in microstructure and material composition.

4.2. *Pore network microarchitecture during aging*

We observed an increasing void volume fraction with age. In our experimental set up, higher pore number, not higher pore diameter, accounted for the most of the higher void volume fraction in older subjects. While this is consistent with some earlier works by Kerley (1965) for instance , this seems in contradiction with the repeated observation that most of the age-related increase in porosity can be explained by an increase in pore area, not in pore number (Cooper et al.,

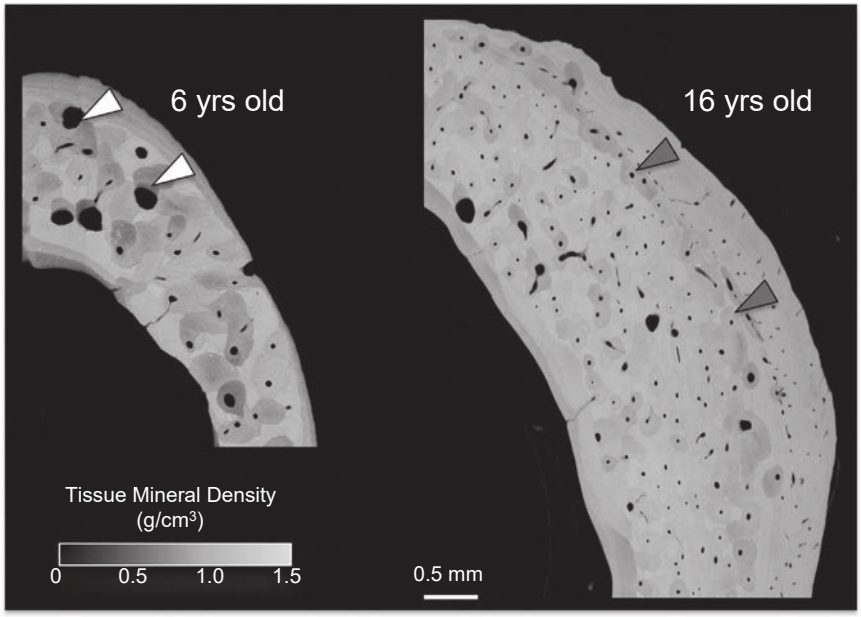

Fig. 3 – Microradiographs of fibula cortical bone cored in the same quadrant from a 6 years old (left panel) and a 16 years old (right panel) boy. White arrows highlight large asymmetric drifting osteons, dark grey arrows highlight smaller symmetric osteons.

2007; Perilli et al., 2015; Thomas et al., 2006). This apparent discrepancy may be explained by the variability in the localization of the VOIs analyzed among the studies. Indeed, the age-related changes in void volume fraction are highly heterogeneous in the bone cross-section and through the thickness of the cortex (Keshawarz and Recker, 1984; Perilli et al., 2015; Zebaze et al., 2010). A recent study by Perilli et al. reported in human subtrochanteric cortical bone that both higher pore number and size accounted for higher void volume fraction in older subject in medial and lateral regions. In the anterior region, the pore diameter, not the pore number, was higher in older subjects compared to the younger ones (Perilli et al., 2015). Across the cortical thickness, with increasing age, bone remodeling becomes particularly vigorous in the inner part of the cortex, the closest to the medullary cavity (Zebaze et al., 2013; Zebaze et al., 2010). In this region, pores not only enlarge focally because of the negative balance, but also coalesce resulting in giant pores and most likely in a local decrease in pore number. This creates a gradient in pore size from the periosteum to the endosteum (Bell et al., 1999; Bell et al., 2001; Chappard et al., 2013; Zebaze et al., 2010).

In the current study, we extruded small cubical samples of compact-appearing cortex excluding the cortico-trabecular junction with its giant pores. In our VOIs, we propose that age related increase in porosity principally originates from an increase in pore number, modestly from an increase in pore size. Indeed, the negative bone balance at the BMU level responsible for canals enlargement is only ~5%; 95% of the bone removed by osteoclasts is refilled representing a deficit of a few microns in regard of the osteonal wall width - a difference unlikely to be detectable using an 8.14 μm voxel size (Qiu et al., 2010). An increase in the number of canals in these confined VOIs suggests an excavation of new canals. This increase in pore number perhaps originates from remodeling initiated upon surfaces of existing BMUs and their branching (Maggiano et al., 2016) or within osteocytes lacunae (Perilli et al., 2015). Indeed, many studies suggest that osteocytes are key regulators of osteoclasts and osteoblasts activities but also may be able to locally remodel the perilacunar bone matrix (Atkins and Findlay, 2012; Bonewald, 2011; Qing et al., 2012; Teti and Zallone, 2009). However, knowing whether new canals can emerge from, or under the control of osteocytes activity needs further research. In addition to increasing the cortical void volume fraction, the excavation of new canals incidentally decreased the average separation between them and that correlated with a lower axial elasticity in traction-compression mode.

It is well documented that the age-related increase in porosity originating from alterations in intracortical remodeling is detrimental for bone strength (Bala et al., 2015; Granke et al., 2011; McCalden et al., 1993). At the tissue level (i.e., mesoscale), variations in cortical porosity explained from 62 to 98% of the variation in compression-tension and shear elastic coefficients (Dong and Guo, 2004; Granke et al., 2011). At the organ level (i.e., macroscale), variations in porosity, explained the majority of the variation in long bones mechanical properties in several human and animal models (Baron et al., 2007; Bousson et al., 2006; Granke et al., 2011; Yeni et al., 1997). However, in these studies, porosity was only regarded as a fraction of void volume and therefore did not provide information about the role of pore network microarchitecture in bone mechanical behavior.

In our population, we noticed that in elderly men and women, changes in pore separation and pore separation intra-individual distribution were correlated with axial tensile-compressive elasticity after accounting for void volume fraction. This new result suggests that for a given porosity, the way this void is fashioned in the bone volume affects significantly bone elasticity. In addition, our results

also displayed that shear elastic coefficients C_{55} and C_{66} were less sensitive to porosity and pore network microarchitecture among adults than observed among growing children. As bone anisotropy is influenced by material properties and structural properties (including osteonal morphology), this could reflect that bone anisotropy may emerge from relatively different structural and compositional variables across life.

Indeed, during growth and ageing the changes in cortical remodeling activity, balance and their consequences on pore network architecture are very distinct. However, with bone tissue age as well as individual's age, matrix properties also vary affecting tissue stiffness. During the last decade, the study of the so-called bone quality or we should say bone qualities has revealed that bone matrix stiffness was also a function of bone mineralization, bone mineral characteristics (crystallinity, maturity, carbonation), arrangement, maturity and cross-linking profile of bone collagen fibrils, all these properties varying with age of both the tissue and the individual (Bala and Seeman, 2015; Malo et al., 2013). The fact that the age-related changes in elastic coefficients are likely multifactorial, with changing in both cortical structure and matrix properties are likely to be the reason why the relationships between some pore network architecture and elastic coefficients were opposite in the present study (e.g., for Po.Sp.SD). Consequently, our understanding of the biomechanical impacts of changes in void volume fraction during pathology or treatments is only a partial improvement in the prediction of bone elasticity using bone imaging and computational modeling of the cortex may need to further consider pore network microarchitecture and regional heterogeneity (Granke et al., 2011; Hellmich et al., 2004). Studying the relative contributions of structural and material properties in age-related changes in mechanical properties will be the very objective of our future studies.

4.3. Strengths and limitations

A strength of the study was the use of a high-resolution imaging modality combined with relevant image processing in assessing bone microstructure *in vitro*. In addition, assessments were performed in site-matched samples of a long bone in growing children and adults. This study is the first to offer an analysis of the 3D microarchitecture of the pore network in growing children in a long bone. Indeed, our knowledge of growth-related changes in cortical porosity comes from histologic studies in iliac crest samples, an irregular and non-load-bearing bone site that rarely fractures (Rauch et al., 2007; Schnitzler, 2015; Schnitzler and Mesquita, 2013; Schnitzler et al., 2009). In addition, elasticity has been evaluated based on the assessment of ultrasonic bulk wave velocities. While this method has been largely used for investigation of bone mechanical properties, it is non-ionizing, non-destructive and provides both axial and one of the few with Resonant Ultrasond Spectroscopy to allow the assessment of shear elastic properties in the three principal directions of bone (Ashman et al., 1984; Espinoza Orias et al., 2009; Granke et al., 2011; Bernard et al., 2013; Remilleux et al., 2015). In addition for such small dimensions, direct mechanical testing are complicated to realize and interpret.

The first limitation of our study was the sample size that precluded the analysis of the sex- and pubertal stage-related differences in the trends we reported with age in both children and adults groups. Bone microarchitecture is known to vary with age with different chronologies in male and female during bone growth or aging (Chen et al., 2010; Khosla et al., 2006; Wang et al., 2010). The trends described in the current paper are coherent with the known age-related changes in bone remodeling and its balance at the BMU level, though. Second, our analyses were performed on VOIs of relatively small size (cubes of 2mm-sides) and consequently were blind to the porosity gradient along the cortical thickness that appears due to the trabecularization of the cortex with ageing. Therefore, it may remain complicated to generalize those results to what happen in different ROIs. However, despite limited to the compact-appearing cortex, our results are relevant in regard of bone strength because the VOIs were the farthest from the neutral axis, i.e., where the effect of bone porosity on strength is at maximum in a bone submitted to bending (Burr, 2010). Third, we used a polychromatic cone-beam micro-CT device, incidentally submitted to beam-hardening. However due to the small size of our specimens and the use of an aluminum filter that reduces beam hardening artefact, no correction was necessary. Fourth, it has been observed that most of the architectural parameters are inter-correlated (Chappard et al., 2013) and may result in multicollinearity. Unfortunately, using non parametric statistics it was not possible to statistically evaluate for potential collinearity among variables. Finally, while pediatric samples were included in our study based on the literature's definition of ‘reference’ for this very population (Rauch et al., 2007), we acknowledge that they were cored following orthopedic issues and results need to be interpreted with cautious.

5. Conclusion

In conclusion, within the limitation of a small sample size, we infer that during both growth and ageing, changes in pore network microarchitecture, that reflects activity and balance of remodeling upon canals surfaces, contributes to cortical bone stiffness. Alterations in this microarchitecture may impact cortical bone mechanical properties independently of the changes in the void volume fraction. While cortical porosity is a strong determinant of bone elasticity, further considering how this void volume fraction is fashioned will improve our ability to predict the changes in strength associated with pathologies and treatments.

Disclosures

The authors declare no competing financial interests. Yohann Bala, Emmanuelle Lefèvre, Jean-Paul Roux, Cécile Baron, Philippe Lasaygue, Martine Pithioux, Valérie Kaftandjian and Hélène Follet declare that they have no conflict of interest related to this work.

Acknowledgement

This research is supported by the French National Research Agency (ANR MALICE Program, under Grant no. BS09-032). We are grateful to Prof. Franck Launay's team, the donors and their legual guardians who consented us to use their samples for investigation. We also acknowledge the technical support of Marine Loubet, Sebastien Rizzo and Florian Montagner.

r e f e r e n c e s

Akkus, O., Polyakova-Akkus, A., Adar, F., Schaffler, M.B., 2003. Aging of microstructural compartments in human compact bone. J. Bone Miner. Res. 18, 1012–1019.

Ashman, R.B., Cowin, S.C., Van Buskirk, W.C., Rice, J.C., 1984. A continuous wave technique for the measurement of the elastic properties of cortical bone. J. Biomech. 17, 349–361.

Atkins, G.J., Findlay, D.M., 2012. Osteocyte regulation of bone mineral: a little give and take. Osteoporos. Int. 23, 2067–2079.

Bala, Y., Bui, Q.M., Wang, X., Iuliano, S., Wang, Q., Ghasem-Zadeh, A., Rozental, T.D., Bouxsein, M.L., Zebaze, R., Seeman, E., 2015. Trabecular and cortical microstructure and frgaility of the distal radius in women. J. Bone Miner. Res. 30, 621–629.

Bala, Y., Chapurlat, R., Cheung, A.M., Felsenberg, D., Laroche, M., Morris, E., Reeve, J., Thomas, T., Zanchetta, J., Bock, O., Ghasem-Zadeh, A., Djoumessi, R.M., Seeman, E., Rizzoli, R., 2014a. Risedronate slows or partly reverses cortical and trabecular microarchitectural deterioration in postmenopausal women. J. Bone Miner. Res. 29, 380–388.

Bala, Y., Seeman, E., 2015. Bone's Material Constituents and their Contribution to Bone Strength in Health, Disease, and Treatment. Calcif. Tissue Int.

Bala, Y., Zebaze, R., Ghasem-Zadeh, A., Atkinson, E.J., Iuliano, S., Peterson, J.M., Amin, S., Bjornerem, A., Melton 3rd, L.J., Johansson, H., Kanis, J.A., Khosla, S., Seeman, E., 2014b. Cortical porosity identifies women with osteopenia at increased risk for forearm fractures. J. Bone Miner. Res. 29, 1356–1362.

Baron, C., Talmant, M., Laugier, P., 2007. Effect of porosity on effective diagonal stiffness coefficients (cii) and elastic anisotropy of cortical bone at 1 MHz: a finite-difference time domain study. J. Acoust. Soc. Am. 122, 1810.

Bell, K.L., Loveridge, N., Power, J., Garrahan, N., Meggitt, B.F., Reeve, J., 1999. Regional differences in cortical porosity in the fractured femoral neck. Bone 24, 57–64.

Bell, K.L., Loveridge, N., Reeve, J., Thomas, C.D., Feik, S.A., Clement, J.G., 2001. Super-osteons (remodeling clusters) in the cortex of the femoral shaft: influence of age and gender. Anat. Rec. 264, 378–386.

Bernard, S., Grimal, Q., Laugier, P., 2013. Accurate measurement of cortical bone elasticity tensor with resonant ultrasound spectroscopy. J. Mech. Behav. Biomed. Mater. 18, 12–19.

Bjornerem, A., Bui, Q.M., Ghasem-Zadeh, A., Hopper, J.L., Zebaze, R., Seeman, E., 2013. Fracture risk and height: An association partly accounted for by cortical porosity of relatively thinner cortices. J. Bone Miner. Res. 28, 2017–2026.

Bjornerem, A., Ghasem-Zadeh, A., Bui, M., Wang, X., Rantzau, C., Nguyen, T.V., Hopper, J.L., Zebaze, R., Seeman, E., 2011. Remodeling markers are associated with larger intracortical surface area but smaller trabecular surface area: a twin study. Bone 49, 1125–1130.

Bonewald, L.F., 2011. The amazing osteocyte. J Bone Miner. Res. 26, 229–238.

Bousson, V., Le Bras, A., Roqueplan, F., Kang, Y., Mitton, D., Kolta, S., Bergot, C., Skalli, W., Vicaut, E., Kalender, W., Engelke, K., Laredo, J.D., 2006. Volumetric quantitative computed tomography of the proximal femur: relationships linking geometric and densitometric variables to bone strength. Role for compact bone. Osteoporos. Int. 17, 855–864.

Bui, M., Bjornerem, A., Ghasem-Zadeh, A., Dite, G.S., Hopper, J.L., Seeman, E., 2013. Architecture of cortical bone determines in part its remodelling and structural decay. Bone 55, 353–358.

Burr, D.B., 2010. Cortical bone: a target for fracture prevention?. Lancet 375, 1672–1673.

Cadet, E.R., Gafni, R.I., McCarthy, E.F., McCray, D.R., Bacher, J.D., Barnes, K.M., Baron, J., 2003. Mechanisms responsible for longitudinal growth of the cortex: coalescence of trabecular bone into cortical bone. J. Bone Jt. Surg. Am. 85-A, 1739–1748.

Chappard, C., Bensalah, S., Olivier, C., Gouttenoire, P.J., Marchadier, A., Benhamou, C., Peyrin, F., 2013. 3D characterization of pores in the cortical bone of human femur in the elderly at different locations as determined by synchrotron micro-computed tomography images. Osteoporos. Int. 24, 1023–1033.

Chen, H., Zhou, X., Shoumura, S., Emura, S., Bunai, Y., 2010. Age- and gender-dependent changes in three-dimensional microstructure of cortical and trabecular bone at the human femoral neck. Osteoporos. Int. 21, 627–636.

Compston, J., 2011. Age-related changes in bone remodelling and structure in men: histomorphometric studies. J. Osteoporos. 2011, 108324.

Cooper, D.M., Thomas, C.D., Clement, J.G., Turinsky, A.L., Sensen, C.W., Hallgrimsson, B., 2007. Age-dependent change in the 3D structure of cortical porosity at the human femoral midshaft. Bone 40, 957–965.

Currey, J.D., Butler, G., 1975. The mechanical properties of bone tissue in children. J. Bone Jt. Surg. Am. 57, 810–814.

Dong, X.N., Guo, X.E., 2004. The dependence of transversely isotropic elasticity of human femoral cortical bone on porosity. J. Biomech. 37, 1281–1287.

Enlow, D.H., 1962. Functions of the Haversian system. Am. J. Anat. 110, 269–305.

Espinoza Orias, A.A., Deuerling, J.M., Landrigan, M.D., Renaud, J. E., Roeder, R.K., 2009. Anatomic variation in the elastic anisotropy of cortical bone tissue in the human femur. J. Mech. Behav. Biomed. Mater. 2, 255–263.

Granke, M., Grimal, Q., Saied, A., Nauleau, P., Peyrin, F., Laugier, P., 2011. Change in porosity is the major determinant of the variation of cortical bone elasticity at the millimeter scale in aged women. Bone 49, 1020–1026.

Hellmich, C., Ulm, F.J., Dormieux, L., 2004. Can the diverse elastic properties of trabecular and cortical bone be attributed to only a few tissue-independent phase properties and their interactions? Arguments from a multiscale approach. Biomech. Model. Mechanobiol. 2, 219–238.

Hildebrand, T., Ruegsegger, P., 1997. A new method for the model-independent assessment of thickness in three-dimensional images. J. Microsc. 185, 67–75.

Jee, W.S., Frost, H.M., 1992. Skeletal adaptations during growth. Triangle; Sandoz J. Med. Sci. 31, 77–88.

Kerley, E.R., 1965. The microscopic determination of age in human bone. Am. J. Phys. Anthropol. 23, 149–164.

Keshawarz, N.M., Recker, R.R., 1984. Expansion of the medullary cavity at the expense of cortex in postmenopausal osteoporosis. Metab. Bone Dis. Relat. Res. 5, 223–228.

Khosla, S., Riggs, B.L., Atkinson, E.J., Oberg, A.L., McDaniel, L.J., Holets, M., Peterson, J.M., Melton 3rd, L.J., 2006. Effects of sex and age on bone microstructure at the ultradistal radius: a population-based noninvasive in vivo assessment. J. Bone Miner. Res. 21, 124–131.

Kohles, S.S., Martinez, D.A., 2000. Elastic and physicochemical relationships within cortical bone. J. Biomed. Mater. Res. 49, 479–488.

Lefevre, E., Lasaygues, P., Baron, C., Payan, C., Launay, F., Follet, H., Pithioux, M., 2015. Analyzing the anisotropic Hooke's law for the children's cortical bone. J. Mech. Behav. Biomed. Mater. DOI: j.jmbbm.2015.05.013.

Lips, P., Courpron, P., Meunier, P.J., 1978. Mean wall thickness of trabecular bone packets in the human iliac crest: changes with age. Calcif. Tissue Res. 26, 13–17.

Loro, M.L., Sayre, J., Roe, T.F., Goran, M.I., Kaufman, F.R., Gilsanz, V., 2000. Early identification of children predisposed to low peak bone mass and osteoporosis later in life. J. Clin. Endocrinol. Metab. 85, 3908–3918.

Maggiano, I.S., Maggiano, C.M., Clement, J.G., Thomas, C.D.L., Carter, Y., Cooper, D.M.L., 2016. Three-dimensional reconstruction of Haversian systems in human cortical bone using synchrotron radiation-based micro-CT: morphology and quantification of branching and transverse connections across age. J. Anat.http://dxdoi.org/10.1111/joa.12430.

Malo, M.K.H., Rohrbach, D., Isaksson, H., Töyräs, J., Jurvelin, J.S., Tamminen, I.S., Kröger, H., Raum, K., 2013. Longitudinal elastic properties and porosity of cortical bone tissue vary with age in human proximal femur. Bone 53, 451–458.

McCalden, R.W., McGeough, J.A., Barker, M.B., Court-Brown, C.M., 1993. Age-related changes in the tensile properties of cortical bone. The relative importance of changes in porosity, mineralization, and microstructure. J. Bone Jt. Surg. Am. 75, 1193–1205.

Montagner, F., Kaftandjian, V., Farlay, D., Brau, D., Boivin, G., Follet, H., 2015. Validation of a novel microradiography device for characterization of bone mineralization. J. X-ray Sci. Technol. 23, 201–211.

Odgaard, A., 1997. Three-dimensional methods for quantification of cancellous bone architecture. Bone 20, 315–328.

Palacio-Mancheno, P.E., Larriera, A.I., Doty, S.B., Cardoso, L., Fritton, S.P., 2014. 3D assessment of cortical bone porosity and tissue mineral density using high-resolution microCT: effects of resolution and threshold method. J. Bone Miner. Res. 29, 142–150.

Parfitt, A.M., 1994a. Osteonal and hemi-osteonal remodeling: the spatial and temporal framework for signal traffic in adult human bone. J. Cell. Biochem. 55, 273–286.

Parfitt, A.M., 1994b. The two faces of growth: benefits and risks to bone integrity. Osteoporos. Int. 4, 382–398.

Parfitt, A.M., Travers, R., Rauch, F., Glorieux, F.H., 2000. Structural and cellular changes during bone growth in healthy children. Bone 27, 487–494.

Perilli, E., Bala, Y., Zebaze, R., Reynolds, K.J., Seeman, E., 2015. Regional heterogeneity in the configuration of the intracortical canals of the femoral shaft. Calcif. Tissue Int. Epub Ahead of Print.

Qing, H., Ardeshirpour, L., Pajevic, P.D., Dusevich, V., Jahn, K., Kato, S., Wysolmerski, J., Bonewald, L.F., 2012. Demonstration of osteocytic perilacunar/canalicular remodeling in mice during lactation. J. Bone Miner. Res. 27, 1018–1029.

Qiu, S., Rao, D.S., Palnitkar, S., Parfitt, A.M., 2010. Dependence of bone yield (volume of bone formed per unit of cement surface area) on resorption cavity size during osteonal remodeling in human rib: implications for osteoblast function and the pathogenesis of age-related bone loss. J. Bone Miner. Res. 25, 423–430.

Rauch, F., 2012. The dynamics of bone structure development during pubertal growth. J. Musculoskelet. Neuronal Interact. 12, 1–6.

Rauch, F., Travers, R., Glorieux, F.H., 2007. Intracortical remodeling during human bone development–a histomorphometric study. Bone 40, 274–280.

Recker, R., Lappe, J., Davies, K.M., Heaney, R., 2004. Bone remodeling increases substantially in the years after menopause and remains increased in older osteoporosis patients. J. Bone Miner. Res. 19, 1628–1633.

Remilleux, M.C., Ulrich, T.J., Payan, C., Rivière, J., Lake, C.R., Le Bas, P.Y., 2015. Resonant ultrasound spectroscopy for materials with high damping and samples of arbitrary geometry. J. Geophys. Res. Solid Earth 120, 4898–4916.

Robling, A.G., Stout, S.D., 1999. Morphology of the drifting osteon. Cells Tissues Organs 164, 192–204.

Saito, M., Marumo, K., 2010. Collagen cross-links as a determinant of bone quality: a possible explanation for bone fragility in aging, osteoporosis, and diabetes mellitus. Osteoporos. Int. 21, 195–214.

Schaffler, M.B., Burr, D.B., 1988. Stiffness of compact bone: effects of porosity and density. J. Biomech. 21, 13–16.

Schnitzler, C.M., 2015. Childhood cortical porosity is related to microstructural properties of the bone-muscle junction. J. Bone Miner. Res. 30, 144–155.

Schnitzler, C.M., Mesquita, J.M., 2013. Cortical porosity in children is determined by age-dependent osteonal morphology. Bone 55, 476–486.

Schnitzler, C.M., Mesquita, J.M., Pettifor, J.M., 2009. Cortical bone development in black and white South African children: iliac crest histomorphometry. Bone 44, 603–611.

Seeman, E., 2008. Structural basis of growth-related gain and age-related loss of bone strength. Rheumatol. Oxf. J. 47 (Suppl. 4) iv2-8.

Seeman, E., Delmas, P.D., 2006. Bone quality–the material and structural basis of bone strength and fragility. New Engl. J Med. 354, 2250–2261.

Teti, A., Zallone, A., 2009. Do osteocytes contribute to bone mineral homeostasis? Osteocytic osteolysis revisited. Bone 44, 11–16.

Thomas, C.D., Feik, S.A., Clement, J.G., 2006. Increase in pore area, and not pore density, is the main determinant in the development of porosity in human cortical bone. J. Anat. 209, 219–230.

Ulrich, D., van Rietbergen, B., Laib, A., Ruegsegger, P., 1999. The ability of three-dimensional structural indices to reflect mechanical aspects of trabecular bone. Bone 25, 55–60.

Ural, A., Vashishth, D., 2014. Hierarchical perspective of bone toughness-from molecules to fracture. Int. Mater. Rev. 59, 245–263.

Vedi, S., Compston, J.E., Webb, A., Tighe, J.R., 1983. Histomorphometric analysis of dynamic parameters of trabecular bone formation in the iliac crest of normal British subjects. Metab. Bone Dis. Relat. Res. 5, 69–74.

Wang, Q., Wang, X.F., Iuliano-Burns, S., Ghasem-Zadeh, A., Zebaze, R., Seeman, E., 2010. Rapid growth produces transient cortical weakness: a risk factor for metaphyseal fractures during puberty. J. Bone Miner. Res. 25, 1521–1526.

Yeni, Y.N., Brown, C.U., Wang, Z., Norman, T.L., 1997. The influence of bone morphology on fracture toughness of the human femur and tibia. Bone 21, 453–459.

Yeni, Y.N., Norman, T.L., 2000. Fracture toughness of human femoral neck: effect of microstructure, composition, and age. Bone 26, 499–504.

Zebaze, R., Ghasem-Zadeh, A., M'bala, A., Seeman, E., 2013. A new method of segmentation of compact-appearing, transitional and trabecular compartments and quantificatino of cortical porosity from high resolution peripheral quantitative computed tomographic images. Bone 54, 8–20.

Zebaze, R.M., Ghasem-Zadeh, A., Bohte, A., Iuliano-Burns, S., Mirams, M., Price, R.I., Mackie, E.J., Seeman, E., 2010. Intracortical remodelling and porosity in the distal radius and post-mortem femurs of women: a cross-sectional study. Lancet 375, 1729–1736.